Journal of Power Sources xxx (2014) 1–7

Contents lists available at ScienceDirect

Journal of Power Sources

journal homepage: www.elsevier.com/locate/jpowsour

# Nanostructured tin–carbon/ $LiNi_{0.5}Mn_{1.5}O_4$ lithium-ion battery operating at low temperature

Q1 Giuseppe Antonio Elia [a], Francesco Nobili [b], Roberto Tossici [b], Roberto Marassi [b], Alberto Savoini [c], Stefania Panero [a], Jusef Hassoun [a, *]

[a] Sapienza University of Rome, Chemistry Department, P.zza Aldo Moro 5, 00185 Rome, Italy
[b] School of Science and Technology, University of Camerino, Via S. Agostino, 1, I-62032 Camerino, Italy
[c] Istituto ENI Donegani, Via Fauser 4, Novara 28100, Italy

## HIGHLIGHTS

- An advanced lithium ion battery operating at low temperature is reported.
- The battery employs nanostructured Sn–C anode and high voltage $LiNi_{0.5}Mn_{1.5}O_4$ cathode.
- The electrolyte is based on a $LiPF_6$ salt dissolved in EC-DEC-DMC mixture.
- The cell has excellent behavior in terms of capacity and cycle life.
- The 4.3 V-cell operates at −5 °C over 200 cycles, with capacity of 105 mAh $g^{-1}$.

## ARTICLE INFO

*Article history:*
Received 10 August 2014
Received in revised form
21 October 2014
Accepted 27 October 2014
Available online xxx

*Keywords:*
Sn-C/$LiNi_{0.5}Mn_{1.5}O_4$
High-voltage
Lithium-ion battery
Low temperature

## ABSTRACT

An advanced lithium ion battery using nanostructured tin–carbon lithium alloying anode and a high voltage $LiNi_{0.5}Mn_{1.5}O_4$ spinel-type cathode is studied, with particular focus to the low temperature range. The stable behavior of the battery is assured by the use of an electrolyte media based on a $LiPF_6$ salt dissolved in EC-DEC-DMC, i.e. a mixture particularly suitable for the low temperature application. Cycling tests, both in half cells and in full lithium ion battery using the Sn–C anode and the $LiNi_{0.5}Mn_{1.5}O_4$ cathode, performed in a temperature range extending from room temperature to −30 °C, indicate that the electrode/electrolyte configuration here adopted may be suitable for effective application in the lithium ion battery field. The full cell, cycled at −5 °C, shows stable capacity of about 105 mAh $g^{-1}$ over more than 200 charge–discharge cycles that is considered a relevant performance considering the low temperature region.



## 1. Introduction

High energy, rechargeable lithium ion batteries are presently attracting increasing interest in view of the rapid development of renewable energy plants and the electric vehicles market. Discontinuous sources, such as solar and wind, require low cost side-systems capable to efficiently store energy, while EVs need satisfactory driving range and high safety levels, hence high performance batteries. The achievement of these severe targets so far required the need of radical changes in the lithium ion battery components, e.g. from conventional graphite anode, $LiCoO_2$ cathode and carbonate based electrolytes [1] to new-chemistry electrodes and electrolytes, characterized by high capacity, low cost and enhanced safety level. Among the anodes, lithium alloying electrodes, such as tin and silicon, revealed the most promising characteristics in terms of high theoretical capacity, i.e. of about 1000 and 4000 mAh $g^{-1}$, respectively, vs. 370 mAh $g^{-1}$ of the graphite anode, low cost and intrinsic safety content [1,2]. However, the large volume variation during the electrochemical alloying de-alloying process, that induces the electrode disintegration with consequent loss of the active material and rapid cell fading, so far hindered the use of Li-alloying electrode in lithium battery. This issue has been recently addressed by incorporating tin or silicon nanoparticles in carbon matrixes of various structures to obtain *nanostructured composites* characterized by enhanced properties in terms of capacity and cycling stability [2–8]. Nanostructured Li-alloy composites are characterized by several advantages in respect to graphite anode in lithium ion battery. Graphite shows, in

* Corresponding author.
*E-mail address:* jusef.hassoun@uniroma1.it (J. Hassoun).

http://dx.doi.org/10.1016/j.jpowsour.2014.10.144
0378-7753/

fact, issues associated with material exfoliation during cycling affecting the full cell stability and safety content. Furthermore, common graphite anode generally shows low capacity at the lower temperature regimes [9]. Among the cathode materials, high voltage lithium transition metal oxides, i.e. $LiM_2O_4$, with spinel-structure triggered large interest due to the high power and energy density compared with standard lithium cobalt oxide electrode [10]. Among these cathode materials, $LiNi_{0.5}Mn_{1.5}O_4$ has been considered the most promising candidate for application in a lithium ion battery of increased energy content. This electrodes is, in fact, characterized by a working potential as high as 4.8 V vs. Li/$Li^+$ and a theoretical specific capacity of 147 mAh $g^{-1}$, with corresponding theoretical energy density of 700 Wh/kg, i.e. value 40% higher than that of the conventional $LiCoO_2$ cathode [11,12]. Furthermore, the efficient use of the lithium ion battery in a wide temperature range appeared crucial factor in determining its effective diffusion. Particular attention has been devoted to the study of the $LiNi_{0.5}Mn_{1.5}O_4$ cathode behavior at the high temperature levels, this in view of possible hazards due to an increased reactivity of the high-voltage cathode with the electrolyte media. Meanwhile, $LiNi_{0.5}Mn_{1.5}O_4$ electrode may suffer from low cycle life and remarkable self-discharge at the higher temperatures due to side reactions and increased solubility of the manganese in the electrolyte [13–17]. New electrolyte compositions suitable for the low temperature applications [9,18–22] as well as fast kinetics electrodes [23,24] have been reported in several research papers. Here we report the study of a lithium ion battery using a nanostructured Sn–C anode and a $LiNi_{0.5}Mn_{1.5}O_4$ high voltage cathode in an EC-DEC-DMC-$LiPF_6$ electrolyte, showing a proper electrochemical stability window and designed to maintain its ionic conductivity suitable for battery application until very low temperature level [18]. Hence, the electrode materials have been characterized from room temperature to −30 °C in lithium half cells, and the full lithium ion battery was cycled up to more than 200 cycles at −5 °C. The results demonstrated that the battery may efficiently cycle at low temperature with limited polarization with a working voltage of 4.3 V and a capacity of about 110 mAh $g^{-1}$ that is 75% of the theoretical value, thus suggesting the suitability of the system for application in the lithium ion battery field.

## 2. Experimental

The synthesis of the Sn–C composite material was performed by impregnating a resorcinol formaldehyde gel by a tin organometallic precursor, i.e. terbutylphenyl-tin, followed by annealing under Ar/$H_2$ 5% for 2 h at 700 °C, as described in detail elsewhere [25,26]. The $LiNi_{0.5}Mn_{1.5}O_4$ cathode was obtained by a wet chemistry synthesis route from $LiNO_3$, $Ni(NO_3)_2 \cdot H_2O$ and $Mn(NO_3) \cdot H_2O$, following a procedure reported in previous paper [27]. Both the Sn–C anode and the $LiNi_{0.5}Mn_{1.5}O_4$ cathode materials were synthesized in our laboratory in a two grams scale.

The conductivity Arrhenius plot of the 1 M solution of $LiPF_6$ in EC:DEC:DMC 1:1:1 (LP71, Merck), selected considering its good behavior at the low temperatures, was performed using a Metrohm platinum blocking electrode cell, having a cell constant of 0.98 $cm^{-1}$. The conductivity cell was immersed in a sealed glass vial, filled by the electrolyte. The resistance of the cell was measured by electrochemical impedance spectroscopy, employing a Biologic VSP potentiostat, within 50 KHz–100 mHz frequency range and applying a 5 mV AC BIAS.

Phase composition of the synthesized materials has been determined by XRD analysis, performed on Rigaku D-max Ultima+ using Cu-K$\alpha_1$ radiation source. Scanning electron microscopy (SEM) was performed using scanning electron microscope Phenom FEI

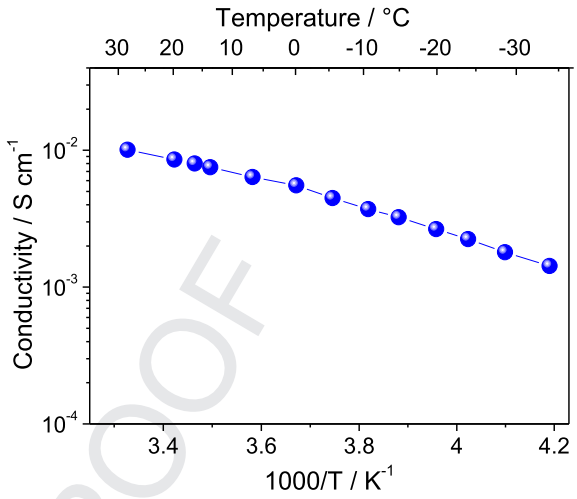


**Fig. 1.** Arrhenius plot of the 1 M solution of $LiPF_6$ in EC:DEC:DMC 1:1:1 (LP71, Merck).

and transmission electron microscopy (TEM) by using a JEOL JSM 7600F instrument.

The Sn/C ratio of the composite was investigated by thermogravimetry (TGA mod. METTLER TOLEDO TGA/SDTA851$^e$ in air flux of 60 ml/min), and by elemental analysis (Fisons EA1108CHNSO combustion elemental analyzer). The results (here not reported) show a Sn:C ratio of 35:65.

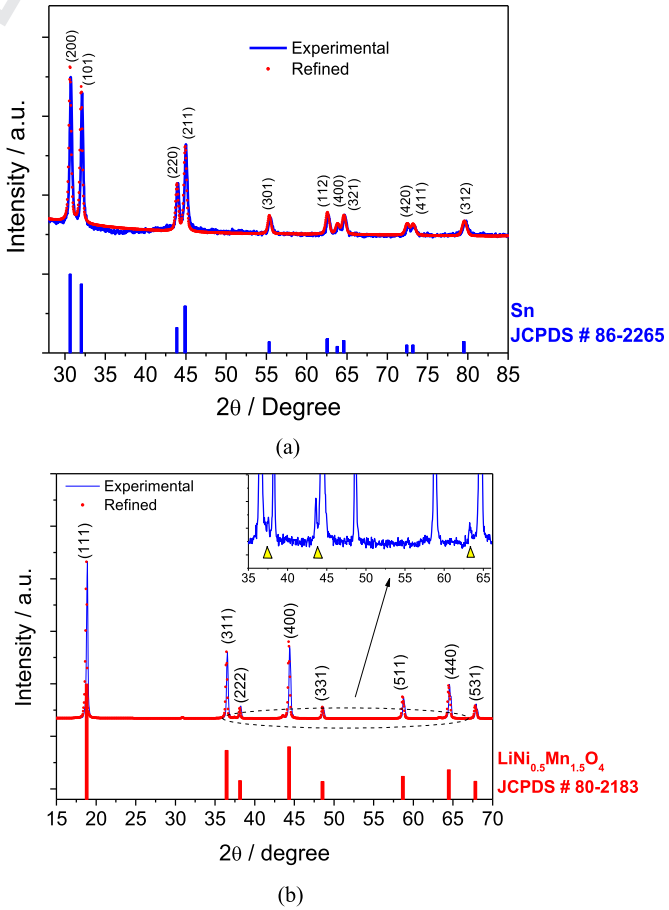


**Fig. 2.** X ray diffraction pattern (XRD) of the Sn–C composite (a) and of the $LiNi_{0.5}Mn_{1.5}O_4$ powder and, in inset, magnification of the diffraction patterns within 35°–65° 2$\theta$ value (b).



Please cite this article in press as: G.A. Elia, et al., Journal of Power Sources (2014), http://dx.doi.org/10.1016/j.jpowsour.2014.10.144

The electrodes were prepared by doctor-blade deposition on a copper foil current collector for the Sn–C composite and aluminum foil for the $LiNi_{0.5}Mn_{1.5}O_4$, using a slurry composed of 80% active material, 10% PVdF (6020, Solef Solvay) as binder and 10% SP carbon (Timcal) as electron conductor additive, dispersed in N-methyl-2-pyrrolidinione (NMP, Aldrich). The obtained film was dried in a vacuum oven for several hours. The active mass loading was of the order of 3 mg $cm^{-2}$ for the anode and of 5 mg $cm^{-2}$ for the cathode material.

The electrochemical measurements were performed by using T-type, Swagelok polypropylene cells, equipped with stainless steel (SS306) current collectors. Lithium cells were assembled in order to evaluate the temperature-dependent behaviors of the two electrode materials, by using Sn–C and $LiNi_{0.5}Mn_{1.5}O_4$ as working electrodes, while metal lithium disks were used as counter and reference electrodes. The lithium-ion cell was assembled by coupling Sn–C and $LiNi_{0.5}Mn_{1.5}O_4$ electrodes as anode and cathode, respectively. Prior to full cell preparation, the first cycle irreversible capacity of the Sn–C anode was reduced by direct contact with a lithium foil, wet by a 1 M $LiPF_6$ EC:DME 1:1 electrolyte solution, for 30 min, under a pressure of 0.4 kg $cm^{-2}$, as already described in a previous paper [28]. The full cell was cathode limited; considering the Sn–C and LMNO loading, i.e. 3 mg $cm^{-2}$ and 5 mg $cm^{-2}$, respectively, and the theoretical capacity of Sn–C and LNMO, i.e. 400 mAh $g^{-1}$ and 148 mAh $g^{-1}$, respectively, the negative to positive ratio (N/P) of the full cell was about 1.6.

For all the cells investigated the electrolyte was a 1 M solution of $LiPF_6$ in EC:DEC:DMC 1:1:1 (LP71, Merck) soaked in a glass-fiber separator (Whatman®). The cells were assembled in an Ar-filled dry-box with $O_2$ and $H_2O$ contents below 10 ppm. Galvanostatic cyclization between 0.01 and 2 V for the Sn–C lithium cell and between 3 and 5 V for the $LiNi_{0.5}Mn_{1.5}O_4$ lithium cell were carried out with a VMP2/Z multi-channel galvanostat-potentiostat (Bio-Logic, France). The galvanostatic cycling of the lithium ion cell was performed using Maccor Series 4000 Battery Test System in the 2.5–4.9 V voltage range.

## 3. Results and discussion

The EC:DEC:DMC 1:1:1, 1 M $LiPF_6$ electrolyte is selected due to its good conductivity at the low temperatures, that is a suitable characteristic for battery applications [18]. Fig. 1, reporting the Arrhenius plot of the electrolyte, shows a conductivity value ranging from $1*10^{-2}$ S $cm^{-1}$ at 30 °C to $1*10^{-3}$ S $cm^{-1}$ at −30 °C, i.e. high values assuring the efficient operation of the lithium ion cells. The successful use of the ternary or quaternary electrolyte system for low-T operative lithium ion battery were already been demonstrated in previous papers [9,21,22]. Here, we characterized the Sn–C nanostructured anode and the $LiNi_{0.5}Mn_{1.5}O_4$ cathode in the same temperature range.

Prior to use, the anode and the cathode have been characterized in terms of structure and morphology. The diffraction pattern reported in Fig. 2a shows reflections that can be indexed to metal Sn (JCPDS # 86-2265), while no evidence of SnO or $SnO_2$ can be detected, thus revealing a proper synthesis conditions that are generally reflected in an optimized behavior of the material in lithium cell, both in terms of high capacity retention and of low charge–discharge polarization [25–27]. The Rietveld refinement of the Sn–C diffraction pattern reveals an $I4_1/amd$ space group and average crystallite size of about 50 nm.

The diffraction pattern of the $LiNi_{0.5}Mn_{1.5}O_4$ reported in Fig. 2b fits well with the structure expected by a disordered spinel framework (JCPDS # 80-2183), characterized by a cubic space group (Fd-3m) that is generally obtained following the synthesis condition used in this work (i.e. 800 °C) [27,29]. Furthermore, the Rietveld refinement confirms the Fd-3m space group and indicates a

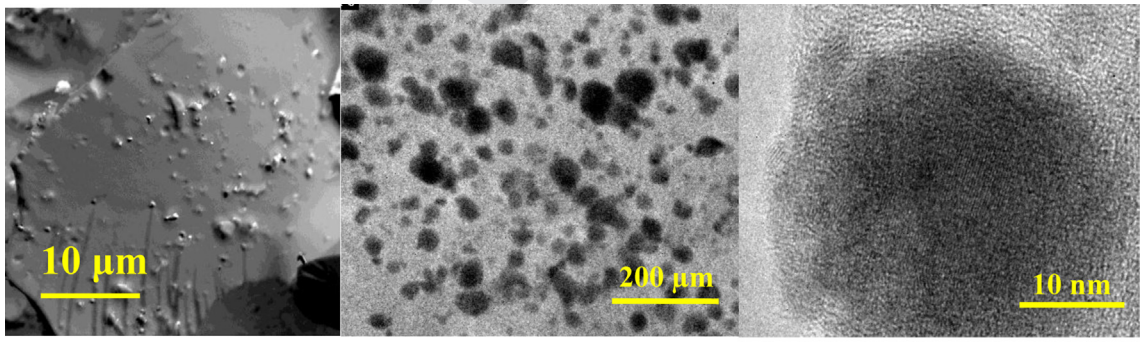


(a)

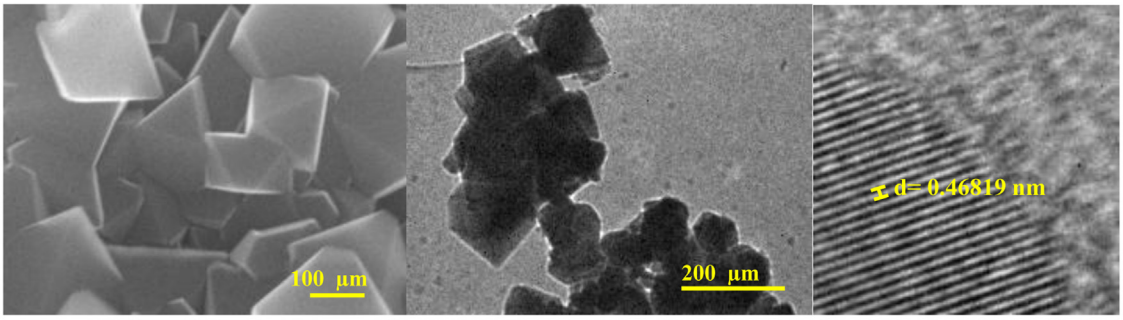


(b)

**Fig. 3.** Scanning electron microscopy images SEM, Bright-field TEM and high-resolution HRTEM images of the Sn–C composite (a) and of the $LiNi_{0.5}Mn_{1.5}O_4$ (b).

Please cite this article in press as: G.A. Elia, et al., Journal of Power Sources (2014), http://dx.doi.org/10.1016/j.jpowsour.2014.10.144

crystallite size of the order of 150 nm [30]. To be noticed that the disordered cubic, Fd3m phase here obtained is expected to have enhanced electrochemical performances in respect to the ordered $P4_332$ one that is generally obtained at lower temperature due its higher electronic conductivity and lithium diffusion coefficient [31,32]. The evaluation of the (311) to (400) peak intensity ratio ($I_{(311)}/I_{(400)}$) of the LMNO indicates a value as high as 0.97, thus suggesting the stability of the cubic structure as reported by literature paper [33]. However, the use of the higher temperature level may cause the formation of minor amount of $Li_xNi_{1-x}O$ impurity (Fm-3m space group) as evidenced by the inset magnification of Fig. 2b marked by yellow (in the web version) triangles [34]. The Rietveld refinement of the pattern allowed the evaluation of the impurity amount, resulting to be of the order of 1.5%.

The morphology of the composite electrode materials has been characterized by scanning electron microscopy (SEM) and transmission electron microscopy (TEM). The SEM image of the Sn–C composite reported in Fig. 3a shows a micrometric carbon matrix trapping tin particles with size ranging from 30 to 70 nm, clearly revealed by the Bright-field TEM and high-resolution TEM images, respectively, and in agreement with the size obtained by XRD refinement. This composite morphology ensures contemporary acceptable tap density, as by the micro-size of the composite and optimized cycling performance, in view of the reduction of the mechanical stress of the nano-sized tin during the Li-alloying process assured by the carbon matrix [25,26,35]. Recently published results [25,26,35] evidenced that the amorphous carbon matrix of the Sn–C composite is characterized by a reversible capacity of the order of 100 mAh $g^{-1}$. Considering the Sn to C ratio of 35:65 (see Experimental section) and the specific capacity associated with the Sn and C, i.e. 993 mAh $g^{-1}$ and 100 mAh $g^{-1}$, respectively, the composite is expected to deliver a reversible capacity of about 400 mAh $g^{-1}$. Fig. 3b reports the morphological characterization of the $LiNi_{0.5}Mn_{1.5}O_4$, spinel-type cathode, by means of SEM and TEM. The SEM image reveals micrometric aggregation of crystals with size ranging from 100 nm to 200 nm, while the high resolution TEM image shows in detail the particles as well as the [111] lattice fringe with plane distance of 0.46819 nm, that is well matching the results obtained by the XRD (0.472023 nm). This particular morphology is known to reflect in an optimized behavior of the electrode in terms of cycling stability, low polarization and high-rate capability.

In order to evaluate the performance of the selected materials at various cycling conditions, lithium cells using the composite Sn–C or the $LiNi_{0.5}Mn_{1.5}O_4$ electrode and the EC:DEC:DMC-based electrolyte have been assembled and galvanostatically cycled at different charge/discharge current rates, i.e. at C/4, C/2 and 1C, and with a temperature range from 20 to −30 °C. The ternary electrolyte system, i.e. $LiPF_6$ 1 M in EC:DEC:DMC 1:1:1 (LP71 by Merck), has been used in order to overcome kinetic limitations due to increase of solvent viscosity and freezing at the low-T limit [37,38]. Fig. 4a, reporting the cycling behavior of the cell using the Sn–C electrode, evidences during the first discharge, performed at 20 °C using a current of 100 mA $g^{-1}$, the characteristic low coulombic efficiency (of about 45%) due to the irreversible side reaction taking place below 0.8 V, attributed to irreversible reactions of the carbon matrix. These reactions include the expected formation of a solid electrolyte interphase (SEI) film [39,40], the reaction of eventual synthesis residuals in the Sn–C composite [25], the eventual irreversible lithium insertion in reticular defects, pores, cavities [35], and the introduction of C–H functionalities [41–43]. During the subsequent cycles the material shows increased efficiency, i.e. ranging from 98 to about 100%, and a reversible capacity of about 400 mAh $g^{-1}$, which is mainly due to the lithium–tin electrochemical alloying process, with minor contribution of the amorphous carbon matrix [25,26]. Furthermore, Fig. 4a and shows that the Sn–C electrode has a satisfactory rate capability considering that it keeps the 70% of its steady state capacity at a current of 400 mA $g^{-1}$, i.e. 1C-rate, at 20 °C. As expected, the capacity of the Sn–C electrode is reduced at the lower temperatures. The cell efficiency appears affected by temperature and current and,

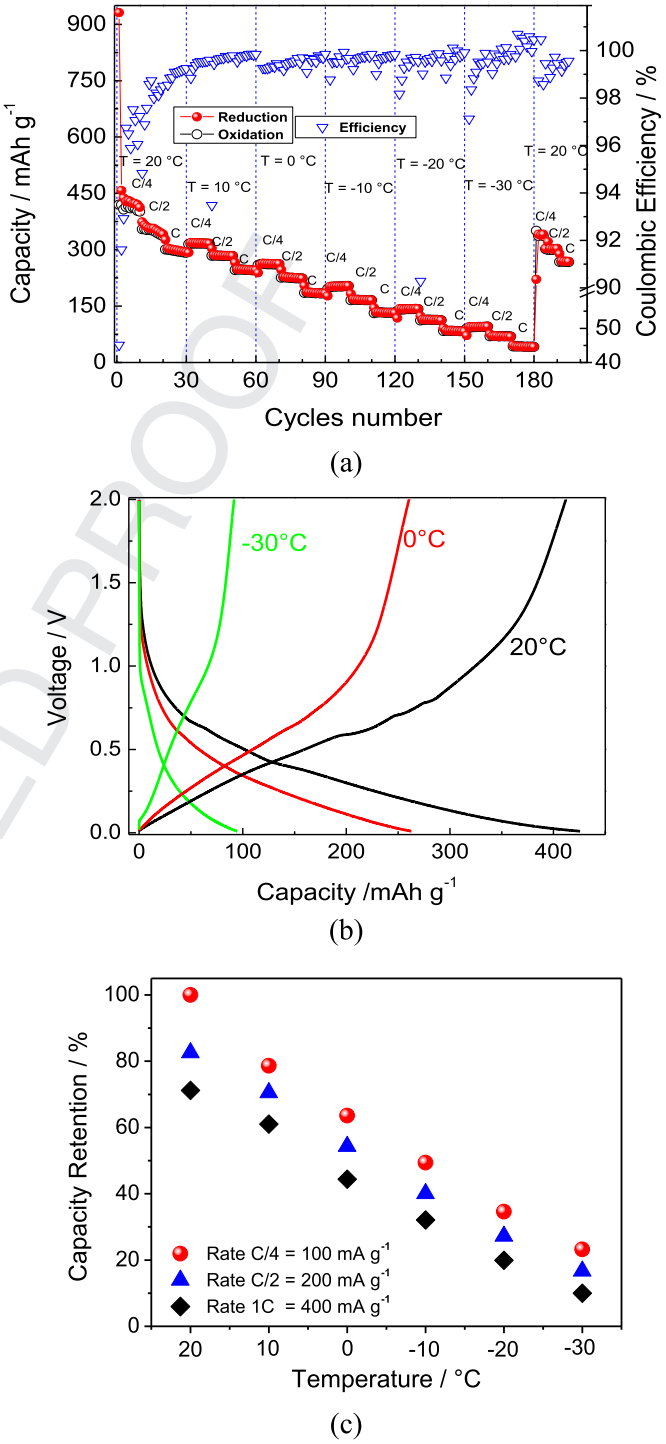


**Fig. 4.** (a) Cycling performance of the lithium cell using the Sn–C composite as the working electrode performed at various current (100, 200, 400 mA $g^{-1}$) and at various temperature (20, 10, 0, −10, −20, −30 °C), (b) voltage profile of the lithium cell using the Sn–C composite as the working electrode performed at 100 mA $g^{-1}$ at 20 °C, 0 °C, −30 °C, and (c) capacity retention of the Sn–C electrode in respect to the steady state value of 400 mAh $g^{-1}$ at the various currents and temperatures.

occasionally, assumes values slightly exceeding 100%, as most likely due to a residual charge accumulation in particular at the lower temperature and higher currents. These cycling performances indicate relevant structural stability of the Sn–C electrode upon cycling.

The voltage profiles shown in Fig. 4b reflect the typical signature of the Sn–C electrode, characterized by multi-step plateau associated with the Li–Sn alloying process at the higher temperature (20 °C) that gradually merges into a uniform sloppy profile by decreasing the temperature. The capacity decrease observed at the lower temperatures can be most likely ascribed to an increased polarization of the electrodes, thus hindering the Li–Sn alloying processes and forcing the electrode to reach the lower cut-off potential before the Li uptake by active Sn and C matrix is completed. This increased polarization results in a linear decrease of the capacity by decreasing the temperature, as demonstrated by Fig. 4c reporting the capacity retention of the Sn–C electrode in respect to the steady state value of 400 mAh $g^{-1}$ at the various temperatures. In the most severe conditions, i.e. $T = -30$ °C and at 1C-rate, the electrode retains a residual capacity of 40 mAh $g^{-1}$, that is 10% of the reference capacity, while in the still demanding but less severe condition of −10 °C and C/4-rate, the electrode shows a capacity of 50% of that of the reference, i.e. 200 mAh $g^{-1}$. As a term of comparison, graphite anodes cannot usually exchange any relevant capacity in comparable conditions, i.e. in the $LiPF_6$ 1 M in EC:DEC:DMC 1:1:1 ternary electrolyte system, $T = -30$ °C, $0.01 < E < 1.5$ V, and C/5 C-rate [9,23,24]. Finally, when the cell is set back to the initial conditions ($T = 20$ °C) after 180 cycles, most of the initial capacity is recovered, with values of about 350, 300, 270 mAh $g^{-1}$ at C/4, C/2, 1C charge/discharge rates, respectively, with a capacity retention higher than 80%.

Fig. 5a shows the cycling performance of the $LiNi_{0.5}Mn_{1.5}O_4$ at the various current, i.e. 148, 74 and 37 mA $g^{-1}$, within 20 to −30 °C temperature range. The cell evidences an irreversible capacity as high as 45% during the first cycle, most likely associated to the electrolyte decomposition at the $LiNi_{0.5}Mn_{1.5}O_4$ surface [44]. Following, the efficiency rises up to about 98% and the cell shows very stable cycling behavior, thus suggesting a stable SEI film formation [35,36]. The relatively high irreversible capacity during the first few cycles may be principally ascribed to the decomposition of EC with consequent formation of a thin film composed by polyethylene-carbonate (PEC), $Li_2CO_3$ and traces of other components, such as $Li_xPF_yO_z$ [43]. The LNMO cell evidences an efficiency affected by temperature and current, i.e. rising up by increasing the current rate and by lowering the temperature and, occasionally, assuming values slightly higher than 100%, this in view of a residual charge accumulation at the lower temperature and higher current already observed for the anode side (see Fig. 4a).

At the steady state conditions the cell delivers a stable capacity of the order of 115 mAh $g^{-1}$ that is about the 80% of the theoretical capacity of $LiNi_{0.5}Mn_{1.5}O_4$ electrode. The system maintains good performance even at very low temperature, with capacity value of 65 mAh $g^{-1}$ at −30 °C using a current of 37 mA $g^{-1}$. The voltage profiles reported in Fig. 5b evidence very limited increase of cell polarization by changing the temperature from 20 °C to 0 °C, while higher, but still acceptable, polarization is observed at −30 °C, with delivered capacity of 60 mAh $g^{-1}$. Details of the capacity retention of the cathode at various rates and temperatures, referred to the steady state capacity of 115 mAh $g^{-1}$, are reported in Fig. 5c. The figure shows good performance even under severe test conditions, with 60% of capacity retention at C/4 current rate and −30 °C as well as at 1C current rate and −10 °C.

Considering the data reported in Figs. 4 and 5, we coupled the Sn–C anode and the $LiNi_{0.5}Mn_{1.5}O_4$ cathode (see Experimental section for cell balance and assembly) together with the EC-DEC-DMC $LiPF_6$ electrolyte in a lithium ion cell, cycled at a C/4 rate versus the cathode weight and at −5 °C. These cycling conditions are selected in order to investigate the cell behavior at acceptable current rate and at a temperature considered usual for winter season, in particular in the north hemisphere. Prior to full cell

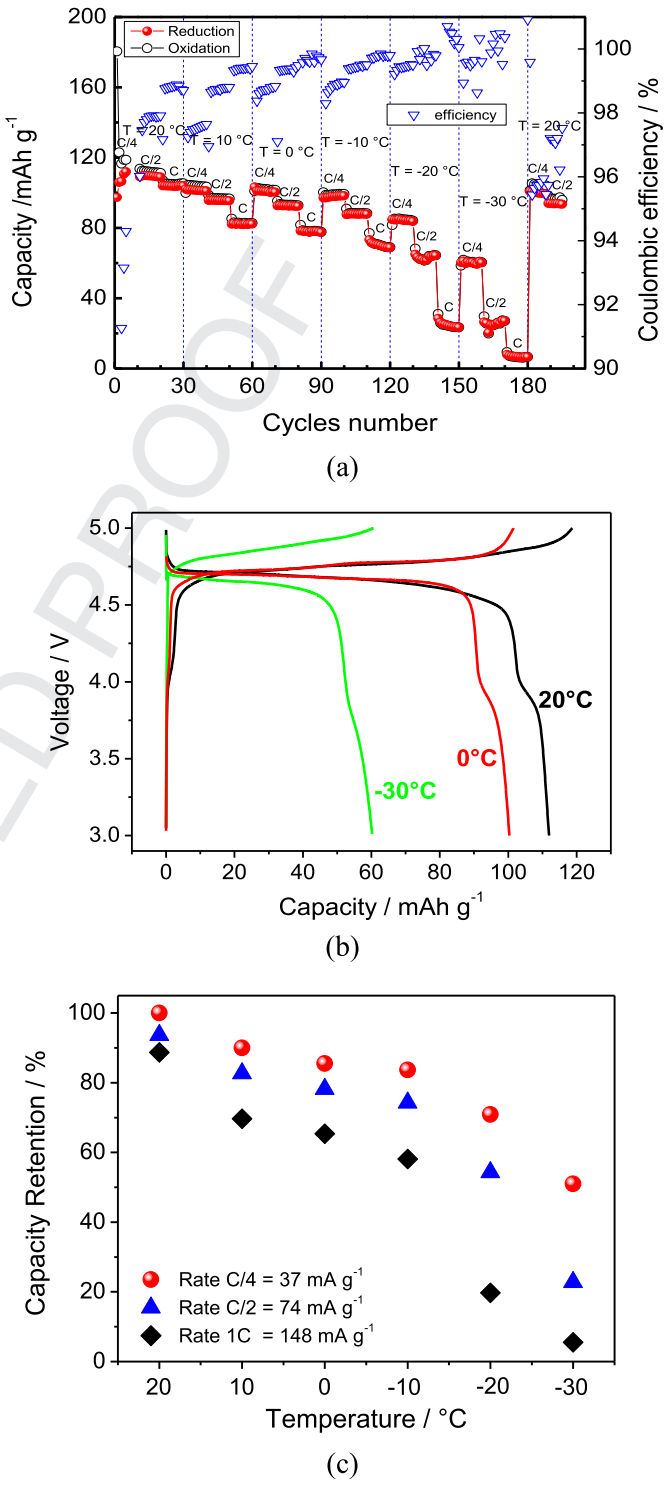


**Fig. 5.** (a) Cycling performance of the lithium cell using the $LiNi_{0.5}Mn_{1.5}O_4$ as the working electrode performed at various current (37, 74, 148 mA $g^{-1}$) and at various temperature (20, 10, 0, −10, −20, −30 °C), (b) voltage signature of the lithium cell using the $LiNi_{0.5}Mn_{1.5}O_4$ as the working electrode performed at 37 mA $g^{-1}$ (C/4) at 20 °C, 0 °C, −30 °C, (c) retention ratio in respect to the steady state value of 115 mAh $g^{-1}$ at the various currents and temperatures.

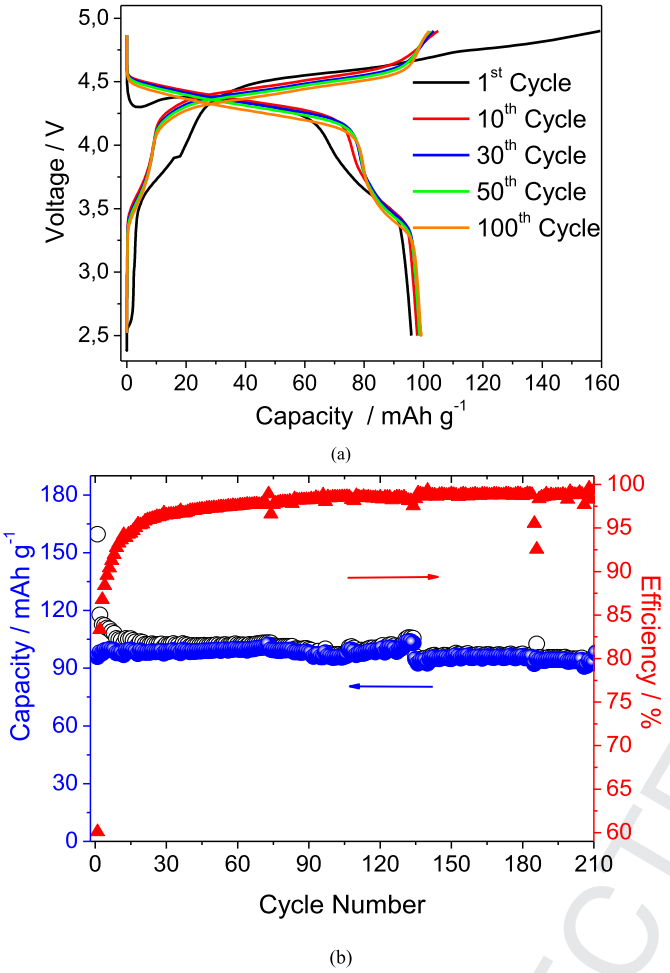


**Fig. 6.** Voltage signature (a) and cycling performance (b) of the lithium ion cell using the Sn–C composite as the anode and $LiNi_{0.5}Mn_{1.5}O_4$ as the cathode. Cycling rate C/4 (37 mA $g^{-1}$ vs cathode), temperature −5 °C, voltage limits 2.5 V–5 V.

assembly, the Sn–C electrode has been activated by direct chemical reduction with lithium metal as described in previous paper [28], in order to remove the first cycle irreversible capacity (see also Fig. 4 discussion). Fig. 6, reporting the voltage profiles (a) and the cycling behavior (b) of the cell, reveals a first cycle (back curve Fig. 6a) characterized by low efficiency, of about 60%, increasing during the following cycles to reach values ranging from 98% to about 100%. The efficiency trend of the full cell may be ascribed to processes already reported for the half cells, such as initial electrolyte decomposition with formation and stabilization of the SEI film and structural reorganization of the electrodes [26,39,40,44]. Upon stabilization, the voltage profiles presented in Fig. 6a reversibly evolve with an average working voltage of about 4.3 V, reflecting the signature expected for the overall electrochemical process:

$$Sn + LiNi_{0.5}Mn_{1.5}O_4 = Li_xSn + Li_{(1-x)}Ni_{0.5}Mn_{1.5}O_4$$

Following the first few cycles, Fig. 6b evidences a remarkable cycling stability extended for more than 200 charge/discharge cycles, with a reversible capacity of the order of 105 mAh $g^{-1}$, that is of about 70% of the theoretical value. Taking into account the data reported in Fig. 6, the energy density of the cell at −5 °C, calculated in respect to the cathode weight, results of the order of 450 Wh $kg^{-1}$, which is expected to reflect in a practical energy density as high as 150 Wh $kg^{-1}$, this considering a theoretical-to-practical conversion factor of 1/3.

## 4. Conclusions

The low temperature performance of a lithium ion cell using a nanostructured Sn–C nanocomposite anode, a $LiNi_{0.5}Mn_{1.5}O_4$ high voltage cathode and EC-DEC-DMC-$LiPF_6$ electrolyte is here reported. The high coulombic efficiency of the studied lithium half-cells and the absence of passivation layer failures demonstrated that the ternary electrolyte designed for low-temperature application may be suitable for application in the Sn–C/$LiNi_{0.5}Mn_{1.5}O_4$ cell. Furthermore, the good performance at the temperature of −5 °C of the full lithium ion cell, both in terms of capacity and of stable charge/discharge cycling, finally confirmed the potential applicability of this particular lithium ion battery configuration at low-temperatures. The aim of the present work was the study cell operating at intermediate-low temperatures. However, proper electrolyte design in order to cover a wide temperature range, including the high temperatures, is certainly required.

## Acknowledgments

The researches leading to these results have received funding from the European Union Seventh Framework Programme (FP7/2007-2013) under grant agreement n° 265644, Project “APPLES Advanced, High Performance, Polymer Lithium Batteries for Electrochemical Storage”. We acknowledge the Istituto ENI Donegani, Novara, Italy, for kindly providing the TEM images.

## References

[1] B. Scrosati, J. Hassoun, Y.-K. Sun, Energy Environ. Sci. 4 (2011) 3287–3295.
[2] John B. Goodenough, Kyu-Sung Park, J. Am. Chem. Soc. 135 (2013) 1167–1176.
[3] A. Magasinski, P. Dixon, B. Hertzberg, A. Kvit, J. Ayala, G. Yushin, Nat. Mater. 9 (2010) 353–358.
[4] N. Liu, Z. Lu, J. Zhao, M.T. McDowell, H.W. Lee, W. Zhao, Y. Cui, Nat. Nanotechnol. 9 (2014) 187–191.
[5] M. Wachtler, M. Winter, J.O.J. Besenhard, Power Sources 105 (2002) 151.
[6] G.A. Elia, S. Panero, A. Savoini, B. Scrosati, J. Hassoun, Electrochim. Acta 90 (2013) 690–694.
[7] K.T. Lee, Y.S. Jung, S.M. Oh, J. Am. Chem. Soc. 125 (2003) 5652–5653.
[8] W.-M. Zhang, J.-S. Hu, Y.-G. Guo, S.-F. Zheng, L.-S. Zhong, W.-G. Song, L.-J. Wan, Adv. Mater. 20 (2008) 1160–1165.
[9] S.S. Zhang, K. Xu, T.R. Jow, Electrochim. Acta 48 (2002) 241–246.
[10] Z. Chenal, D.-J. Lee, Y.-K. Sun, K. Amine, MRS Bull. 36 (2011) 498–505.
[11] R. Santhanam, B. Rambabu, J. Power Sources 195 (2010) 5442.
[12] A. Kraytsberg, Y. Ein-Eli, Adv. Energy Mater. 2 (2012) 922.
[13] D. Aurbach, B. Markovsky, Y. Talyossef, G. Salitra, H.-J. Kim, S. Choi, J. Power Sources 162 (2006) 780–789.
[14] B. Li, L. Xing, M. Xu, H. Lin, W. Li, Electrochem. Commun. 34 (2013) 48–51.
[15] L. Hu, Z. Zhang, K. Amine, J. Power Sources 236 (2013) 175–180.
[16] B. Markovsky, Y. Talyossef, G. Salitra, D. Aurbach, H.-J. Kim, S. Choi, Electrochem. Commun. 6 (2004) 821–826.
[17] X. Wu, X. Li, Z. Wang, H. Guo, J. Wang, P. Yue, J. Solid State Electrochem. 17 (2013) 1029–1038.
[18] E.J. Plichta, W.K. Behl, J. Power Sources 88 (2000) 192–196.
[19] L.F. Xiao, Y.L. Cao, X.P. Ai, H.X. Yang, Electrochim. Acta 49 (2004) 4857–4863.
[20] M.C. Smart, J.F. Whitacre, B.V. Ratnakumar, K. Amine, J. Power Sources 168 (2007) 501–508.
[21] C.-K. Huang, J.S. Sakamoto, J. Wolfenstine, S. Surampudi, J. Electrochem. Soc. 147 (2000) 2893–2896.
[22] S.S. Zhang, K. Xu, T.R. Jow, J. Power Sources 115 (2003) 137–140.
[23] F. Nobili, M. Mancini, S. Dsoke, R. Tossici, R. Marassi, J. Power Sources 195 (2010) 7090.
[24] M. Mancini, F. Nobili, S. Dsoke, F. D'Amico, R. Tossici, F. Croce, R. Marassi, J. Power Sources (2009) 141.
[25] G. Derrien, J. Hassoun, S. Panero, B. Scrosati, Adv. Mater. 19 (2007) 2336.
[26] J. Hassoun, G. Derrien, S. Panero, B. Scrosati, Adv. Mater. 20 (2008) 3169.
[27] P. Reale, S. Panero, B. Scrosati, J. Electrochem. Soc. 152 (2005) A1949.
[28] J. Hassoun, K.-S. Lee, Y.-K. Sun, B. Scrosati, J. Am. Chem. Soc. 133 (2011) 3139.
[29] M. Kunduraci, G.G. Amatucci, J. Electrochem. Soc. 153 (2006) A1345.
[30] M.-L.-P. Le, P. Strobel, C.V. Colin, T. Pagnier, F. Alloin, J. Phys. Chem. Solids 72 (2011) 124–135.

[31] M. Kunduraci, J.F. Al-Sharab, G.G. Amatucci, Chem. Mater. 18 (2006) 3585–3592.
[32] J.-H. Kim, S.-T. Myung, C.S. Yoon, S.G. Kang, Y.-K. Sun, Chem. Mater. 16 (2004) 906–914.
[33] T.F. Yi, Y.R. Zhu, Electrochim. Acta 53 (2008) 3120–3126.
[34] S. Patoux, L. Daniel, C. Bourbon, H. Lignier, C. Pagano, F. Le Cras, S. Jouanneau, S. Martinet, J. Power Sources 189 (2009) 344–352.
[35] J.R. Dahn, T. Zheng, Y. Liu, J.S. Xue, Science 270 (1995) 590.
[36] J. Hassoun, S. Panero, P. Reale, B. Scrosati, Adv. Mater. 21 (2009) 4807.
[37] M.C. Smart, B.V. Ratnakumar, S. Surampudi, J. Electrochem. Soc. 146 (1999) 486.
[38] H.C. Shiao, D. Chua, H.P. Ling, S. Slane, M. Salomon, J. Power Sources 87 (2000) 167.
[39] D. Aurbach, B. Markovsky, M.D. Levi, E. Levi, A. Schechter, M. Moshkovich, Y. Cohen, J. Power Sources 81–82 (1999) 95–111.
[40] D. Aurbach, J. Power Sources 89 (2000) 206–218.
[41] T. Zheng, W.R. McKinnon, J.R. Dahn, J. Electrochem. Soc. 143 (1996) 2137.
[42] N.A. Kaskhedikar, J. Maier, Adv. Mater. 21 (2009) 2664.
[43] M. Winter, K.-C. Moeller, J.O. Besenhard, in: G.-A. Nazri, G. Pistoia (Eds.), Lithium Batteries. Science and Technology, Kluwer, New York, 2004, p. 160.
[44] L. Yang, B. Ravdel, B.L. Luchta, Electrochem. Solid State 13 (2010) A95–A97.



Please cite this article in press as: G.A. Elia, et al., Journal of Power Sources (2014), http://dx.doi.org/10.1016/j.jpowsour.2014.10.144